EUROMECH COLLOQUIUM 509
Vehicle Aerodynamics
External Aerodynamics of Railway Vehicles, Trucks, Buses and Cars
Berlin, Germany, March 24--25, 2009

PIV INVESTIGATION OF THE FLOW FIELD UNDERNEATH A GENERIC HIGH-SPEED TRAIN CONFIGURATION

Mattias Jönsson[*], Johannes Haff[*], Hugues Richard[*], Sigfried Loose[*] and Alexander Orellano[†]

[*]Institute of Aerodynamics and Flow Technology, Department of Technical Flows (AS-TS)
German Aerospace Center (DLR), Bunsenstrasse 10, 37073 Göttingen, Germany
e-mail: Mattias.Joensson@dlr.de, Johannes.Haff@dlr.de, Hugues.Richard@dlr.de, Sigfried.Loose@dlr.de

[†] Center of Competence, Aerodynamics and Thermodynamics
Bombardier Transportation, Am Rathenaupark, 16761 Hennigsdorf, Germany
e-mail: Alexander.Orellano@de.transport.bombardier.com

Keywords: High-Speed Trains, Vehicle Aerodynamics, PIV, Euromech 509.

Abstract. *In this paper a 2C PIV measurement of the flow field underneath a 1:50 generic high-speed train configuration (front car, 2 coaches and tail car) and a smooth generic high-speed train configuration (the same model but without bogies and the bogie cut outs and inter car gaps filled) hauled through a water towing tank at a speed of 4 m/s is presented. The 2C PIV set-up was installed so that the vertical plane (XZ) between the ground and the train, in the centre line of the train, could be measured. The PIV system that was used could measure with an acquisition rate of 10 Hz, at this frequency 6 PIV images of the instantaneous flow field with a distance of 0.4 m from each other were made per run. The total field of view was 0.065 m x 0.025 m (WxH), to cover the entire flow field underneath the train model the position had to be shifted 8 times this was realized with the help of a trigger system. At every position 10 runs were made from which the ensemble average was calculated and reconstructed with the known shift, leading to the average flow field underneath the generic high-speed train configuration. All the presented results in this paper are from the calculated ensemble average.*

The PIV measurement technique was applicable to measure the flow field underneath a down scaled train model in a water towing tank. The generic high-speed train configuration was compared to a full scale measurement. The same structure of the flow field was found for the flow around the head and the tail of the train. The flow field was fully developed at the beginning of the 2nd coach for both configurations. This also agrees with the full scale measurement. To achieve more realistic results in the future the simplified bogies that were used should be replaced with bogies with a higher degree of details. For the comparison between the two measured configurations a clear difference was found, the generic high-speed train configuration had a higher induced velocity underneath the train due to the protruding bogies.

1 INTRODUCTION

The interest in underfloor aerodynamics of high-speed trains has increased in the last years due to the occurrence of several ballast projection incidents (flying ballast stones). Ballast projection correlated with ice/snow packing on the underbelly of the train, which later during travel falls down on the track and dislodges ballast stones, has been known since the beginning of the 1980's [1]. The measure to the snow/ice packing problem was to lower the ballast by around 4 cm beneath the sleepers [2]. In 2003 during a homologation test a ballast projection incident occurred though no winter conditions or foreign objects on the track bed were reported [3]. This was the first ballast projection incident initiated by the induced flow underneath the train. The aerodynamically loads grows quadratic with the train velocity which makes this a problem for high-speed trains. This motivated some of the operators and manufactures in the European railway industry to establish a project named AOA (Aerodynamics in Open Air) were one of the aims were to understand the mechanism of ballast projection. Within this project a full scale measurement was conducted with different types of measurement techniques installed to investigate the aerodynamically loads on the track bed [4]. Measurement techniques installed into the track bed have to be below the Top Of the Rail (TOR) due to safety reasons, hence from TOR and below the aerodynamically loads and the flow field can be measured.

To investigate the entire flow field underneath a train a PIV (Particle Image Velocimetry) measurement [5] on a 1:50 generic high-speed train configuration and a 1:50 smooth generic high-speed train (the same model but without bogies and the bogie cut outs and inter car gaps filled) in a water towing tank was carried out and described in this paper.

2 MEASUREMENT SETUP

2.1 Water Towing Tank Göttingen (WSG)

The 2C PIV measurement presented in this paper was performed in the water towing tank at DLR Göttingen. The water towing tank is an 18x1.1x1.1 m (LxWxH) big steel tank with thick glass window for optical measurements and visualizations see Fig. 1.

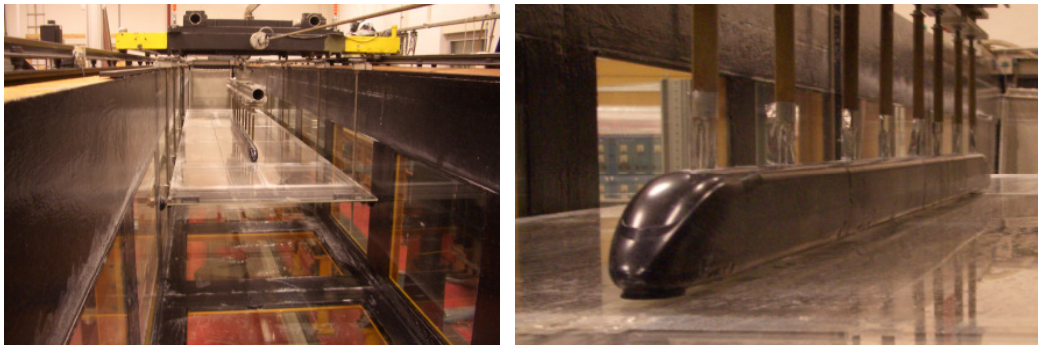

Figure 1: The water towing tank (left) and the generic smooth high-speed train configuration (right).

On the two upper edges of the tank rails for the moving model rig are installed. With the help of a steel cable and an electrical motor (installed outside the channel) the moving model rig can reach speeds up to 5 m/s. For this measurement a speed of 4 m/s was chosen, this corresponds to a Reynolds number of 0.24 Mio with the reference length scale of 3 m divided by the model scale (0.06 m) [6].

The 1:50 train model set (front car, 2 coaches and tail car) was attached to the moving model rig with the help of a long X-profile. Clamped onto the X-profile were 8 NACA 0030

profiles which emerged the train model into the water. The NACA profiles were chosen to minimize the influence of the flow field around the train model and were mounted on top of the roof to keep the flow field underneath the train model as undisturbed as possible. The fact that the NACA profiles might change the properties of the flow field underneath the train are not neglected but are considered as small.

For the correct ground simulation a ground plate was installed in the towing tank with a ground clearance of 0.235 m divided by the model scale (0.0047 m) that is the distance between ground and train wheel [6]. The ground plate was made out of Plexiglas plates mounted onto aluminum profiles, the ground had to be transparent for the light sheet in the 2C PIV set-up.

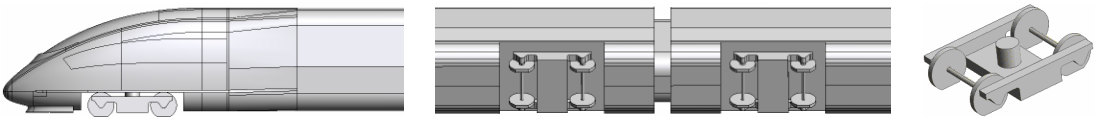

Figure 2: Shows the CAD model of the generic high-speed train configuration, head/tail (left), underbelly (middle) and the simplified bogie (right).

2.2 Particle Image Velocimetry Set-up and Measurement

The 2C PIV set-up that was used is shown in Fig. 3, the laser, light sheet optics and the 2 cameras are all installed outside the channel. The light sheet was so installed that the vertical plane between the ground and the train at the centre line of the train could be measured. The two cameras were installed perpendicular to the light sheet at both sides of the channel, two cameras were used to increase the measurement field or so called field of view, total field of view became 0.065x0.025 m (WxH). The 2 cameras were PCO 1600 cooled digital 14 bit CCD cameras with a resolution of 1600x1200 pixels (WxH), about 450 pixels resolved the gap between the ground and the train.

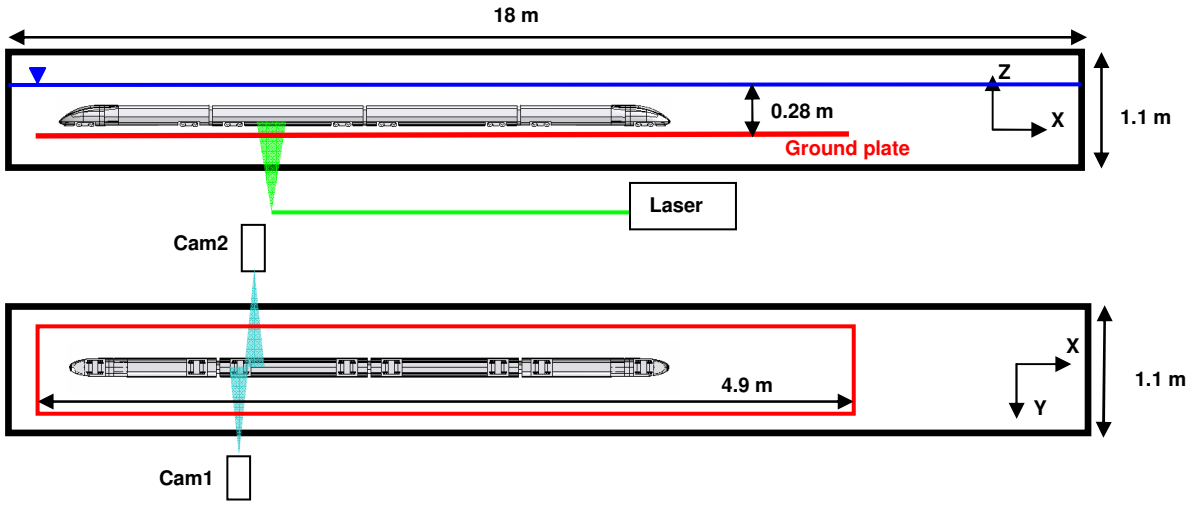

Figure 3: Sketch of the PIV set-up in the water towing tank.

The maximum acquisition rate of the PIV system was 10 Hz, with this frequency it was only possible to sample 6 PIV images with a 0.4 m distance from each other per run. To cover the entire train length (~2.1 m) the position of the train was shifted 8 times, this was done with the help of a trigger system. At every position 10 runs were made to be able to calculate

the ensemble average of the flow field, more over the post-processing of the PIV data will be explained in the next chapter.

3 DATA TREATMENT

3.1 Evaluation of the PIV Data

The major steps in the post processing of the PIV data are listed below.

1) Calculate the flow field with the help of cross-correlation between the PIV images [7].
2) Find the shift between the runs to allocate the exact train positions.
3) Average the overlap between camera 1 and 2 and then shift the data into its right position for every run, thereafter the ensemble average was calculated, see Eq. 1. This was done for the flow field at every position.
4) Use the ensemble average flow field at every position to recreate the entire flow field underneath the train.

$$c(x_j, z_k) = \frac{1}{n}\sum_{i=1}^{n} c_i(x_j, z_k) \tag{1}$$

$$Cu(x,z) = \frac{U(x,z)}{Utrain}, \quad Cw(x,z) = \frac{W(x,z)}{Utrain} \tag{2), (3}$$

For the cross-correlation of the PIV images a multigrid interrogation (grid refinement) was used with a final interrogation window size of 24x24 pixels (0.522x0.522 mm) with an overlap of 75%. This configuration gave about 75 data points over the gap between the train and the ground.

Reference lines were painted on the side of the train to simplify the allocation of the train positions, the shift between the runs were about ±0.0024 m. The lines enhance the accuracy of the ensemble average that was calculated for every position. When the shifts were found the PIV data from camera 1 and camera 2 were interpolated onto a slightly bigger equidistant grid (Δx=0.00013 m, Δz=0.00013 m), the bigger grid made it possible to interpolate all PIV data at one position onto the same grid independent of the magnitude of the shift, and then the overlapping data between camera 1 and camera 2 was averaged. For every position an ensemble average was calculated from the 10 runs, due to the shift between the runs, the ensemble average at the outer edges had a low sample rate and therefore a criteria was used that at least 8 samples out of 10 possible were needed to be defined as valid data. The ensemble average for every position was shifted to its right position and every overlapping region was averaged.

4 RESULTS

The presented results are the ensemble average of the flow field measured at the different positions and then put together to represent the entire flow field underneath the generic high-speed train configuration and the smooth generic high-speed train configuration.

4.1 Flow Field

In Fig. 4 the velocity field for the generic high-speed train configuration is shown in four plots, one for each part of the train set. For the upper plot where the front car is shown the effect of the head can be seen. In front of the head the water (in this case) is pushed in the same direction as the train travels, in 3D the water is pushed away from the head in all direction, this creates a reversal flow area around the head of the front car which can be seen in the plot. The reversal flow area ends shortly after the first bogie on the front car. Thereafter the flow

underneath the train is dragged in the direction of travel. The flow field underneath the train model develops with the train length until the beginning of the 2nd coach where it is fully developed. The flow field for the 2nd coach and the tail car is very similar at the beginning and until the middle of the tail car. The flow field for the second half of the tail car is influenced of the aerodynamics around the tail and that the train ends. The strong influence of the bogie-inter car gap-bogie area can also be seen, which is obviously since the underbelly is completely smooth except for these areas.

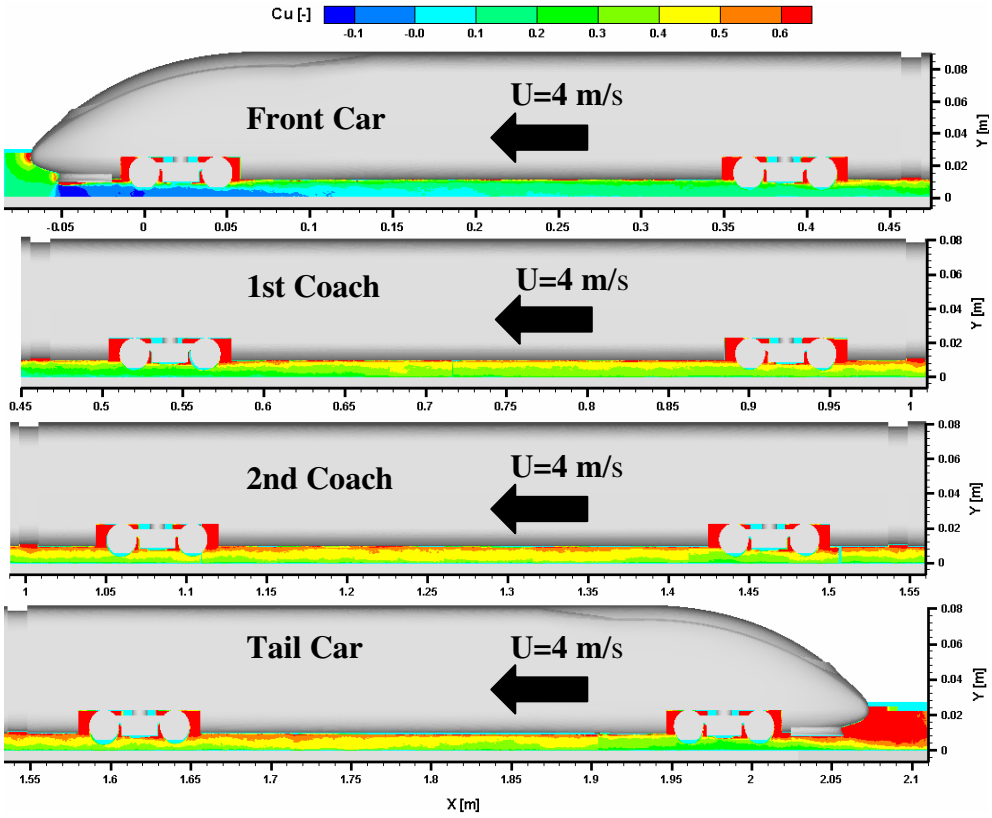

Figure 4: The Cu flow field underneath the generic high-speed train configuration.

In Fig. 5 the flow field for smooth generic high-speed train configuration is shown. At the train head the same phenomena as for the generic high-speed train configuration appears, but for this configuration the reversal flow area is more stretched out along the train length than for the generic high-speed train configuration. Also for this configuration the flow field is fully developed at the beginning of the 2nd coach. The Cu-value underneath the smooth generic high-speed configuration is smaller than for the generic high-speed train configuration, this was expected since the roughness on the underbelly was smaller. The difference between the two configurations shows the influence of the bogie-inter car gap-bogie areas. Thus it is shown that the bogie-inter car gap-bogie areas are the areas to improve to reduce the risk of ballast projection but also a topic for drag reduction of high-speed trains.

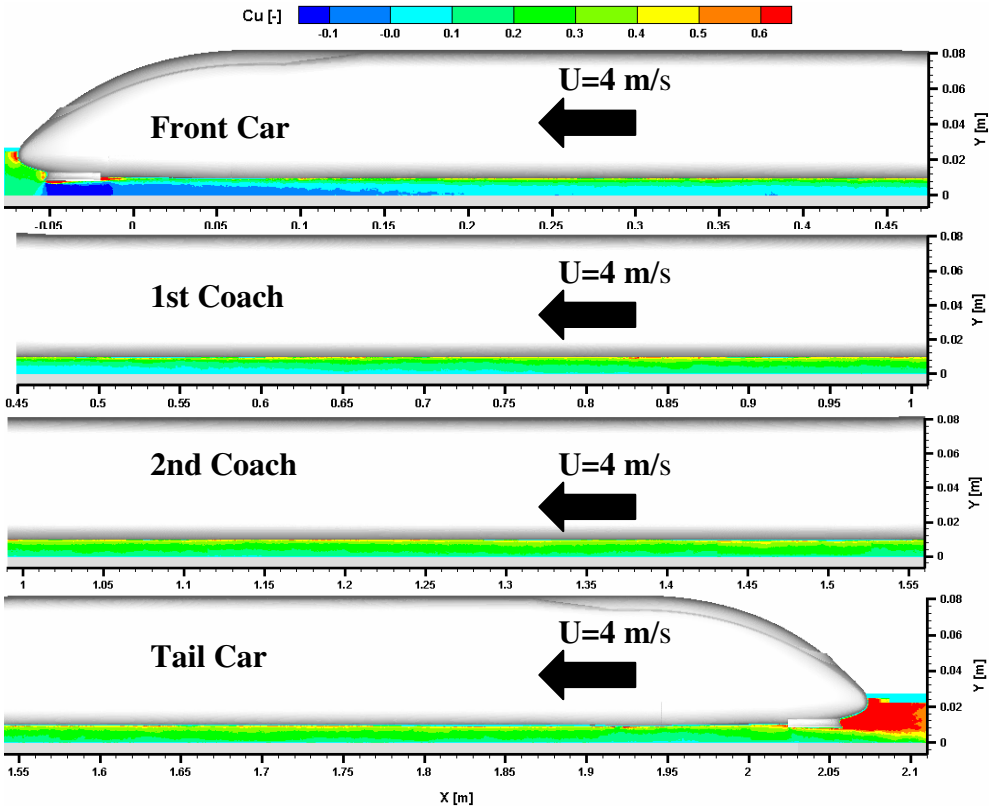

Figure 5: The Cu flow field underneath the smooth generic high-speed train configuration.

Small discrepancies between the coaches and between the two configurations might be hidden in the color scale and therefore data were extracted from the flow fields along the train length at different heights (Z-pos.) for a better comparison.

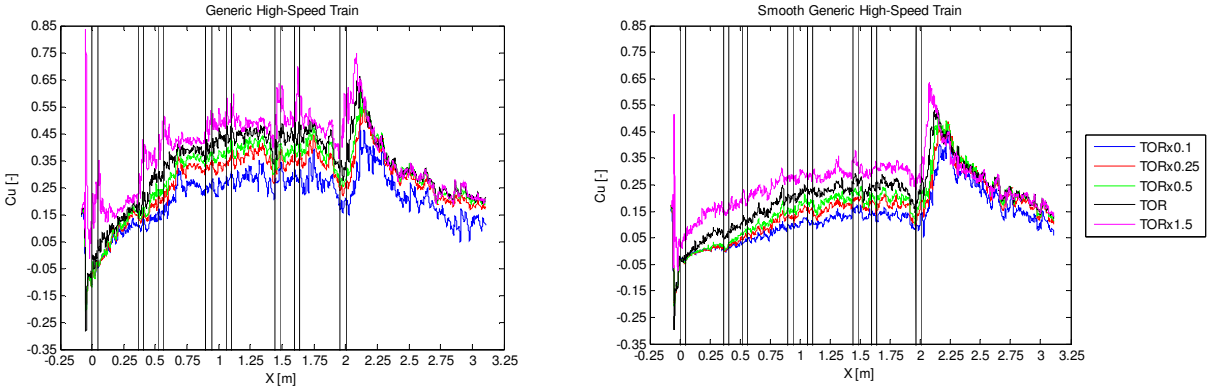

Figure 6: The Cu-value plotted against the train length for the generic high-speed train configuration (left) and the smooth generic high-speed train configuration (right) at different heights (z-pos.). The vertical black lines indicate the positions of the train axles for the generic high-speed train configuration.

The extracted data along the train length for 5 different heights are plotted in Fig. 6. For the smooth generic high-speed train configuration the trend of the curves are very similar, what separates them from each other are the magnitude of the Cu-value. The same trend was also found for the generic high-speed train configuration, except for the height 1.5xTOR (purple curve). For this height the effect of the bogies can easily be seen at every train axle where a peak in the Cu-value is found. The growth of the Cu along the train model length is pretty

constant until the beginning of the 2nd coach where the flow field is fully developed, this applies for both configurations. However the gradient for the front car and the 1st coach is higher for the generic high-speed train configuration than for the smooth generic high-speed train configuration due to the presence of the bogies.

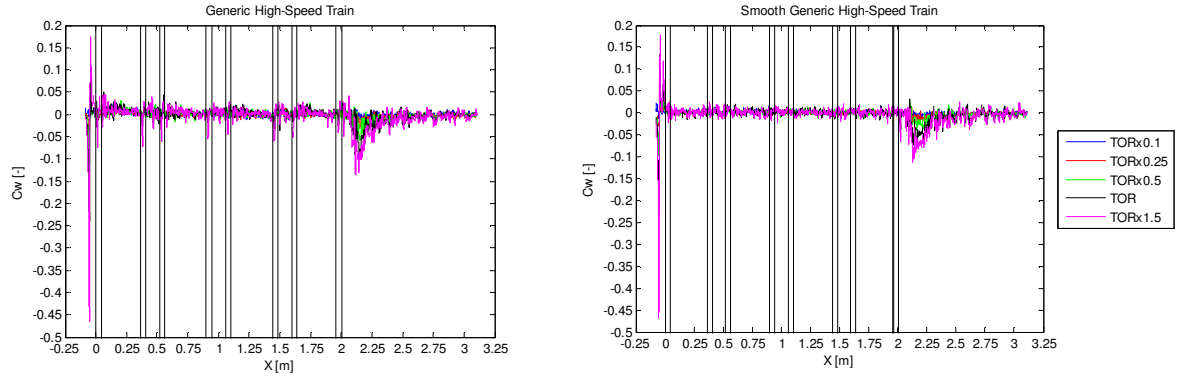

Figure 7: The Cw-value plotted against the train length for the generic high-speed train configuration (left) and the smooth generic high-speed train configuration (right) for different heights (z-pos.). The vertical black lines indicate the positions of the train axles for the generic high-speed train configuration.

In Fig. 7 the normalized vertical velocity (Cw) for the same height as for Cu are plotted. The vertical velocity is dominant at the head and at the tail of the train for both configurations (strongest for the head). There are no protruding objects underneath the smooth generic high-speed train configuration so no vertical velocities are expected, accept for the head and the tail of the train, so the vertical velocity that swings around zero along the train length is considered as noise. However for the generic high-speed train configuration were protruding objects exist (bogies) vertical velocities along the train was found, especially for the height 1.5xTOR (purple curve) which is closest to the train. The Cw peaks with a direction towards the ground found for the height 1.5xTOR is the effect of the protruding bogie frame which is not aligned with the underbelly of the train. Also here the vertical velocity that fluctuates around zero at the middle of the coaches is considered as noise.

For the comparison between the two measured configurations the velocity data at TOR were chosen and plotted in Fig. 8.

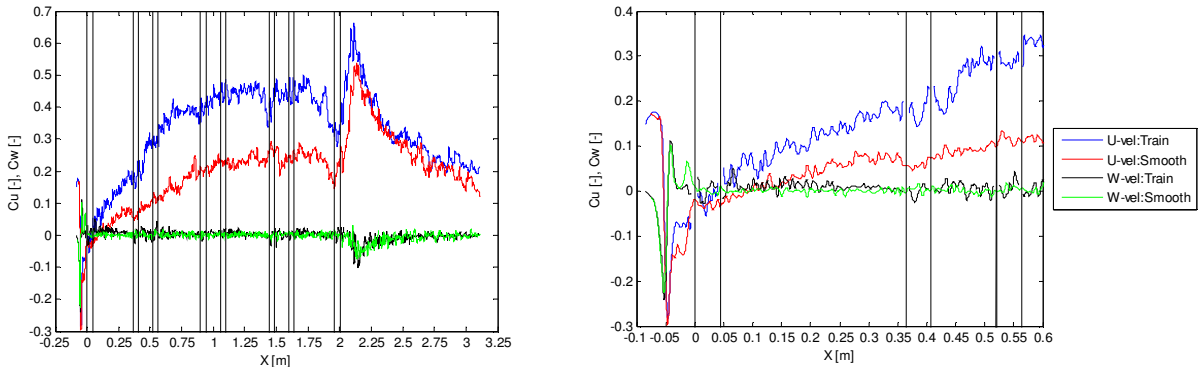

Figure 8: Comparison between the generic high-speed train configuration (Cu: blue and Cw: black) and the smooth generic high-speed configuration (Cu: red and Cw: green). The vertical black lines indicate the positions of the train axles for the generic high-speed train configuration.

In front of the train head no difference can found between the two configurations, it is first shortly before the first bogie where the two configurations deviate from each other. After the

first bogie a clear difference for the Cu between the configurations along the entire train model length can be observed, it is first in the wake of the train model where the Cu value of both configurations comes close to each other again. However for the Cw, differences between the configurations are found around bogie areas which are no surprise since one of the configurations is totally smooth. The same tendencies were also found for the other heights as for TOR. The only difference was found for the data closer to the ground where the configurations first deviate from each other shortly after the fist bogie instead of before due to the distance to the bogies.

In the two tables below the Cu average for the 2nd coach at different heights are shown and compared to each other. The average of the 2nd coach was used, instead of the entire train model length, because the flow field underneath the train model is fully developed at the beginning of the 2nd coach. For the tail car the aerodynamics around the tail and the end of the train model affects the flow field underneath the tail car. Also in [4] the front car and the first coach but also the last coach and the tail car were neglected in the calculation of the train average. For the train model set in this paper the principle in [4] could not be applied and therefore the 2nd coach was chosen.

	Generic High-Speed Train		**Smooth Generic High-Speed Train**	
Height	**Cu [-]**	**Cu/Cu(TOR) [-]**	**Cu [-]**	**Cu/Cu(TOR) [-]**
TOR	0.43833	1	0.23571	1
0.1xTOR	0.27901	0.63653	0.12587	0.53401
0.15xTOR	0.31723	0.72371	0.14545	0.61705
0.25xTOR	0.35306	0.80545	0.16695	0.70826
0.5xTOR	0.38994	0.88959	0.19404	0.82320
0.75xTOR	0.41397	0.94442	0.21441	0.90960
1.25xTOR	0.46315	1.05662	0.26287	1.11520
1.5xTOR	0.49494	1.12915	0.29682	1.25923

Table 1: The average Cu and the Cu normalized by the Cu(TOR) for the 2nd coach at different heights.

In Table 1 the tendency for the average Cu for the 2nd coach can easily be seen, for both configurations the Cu average grows with a decreasing distance to the train model. For the normalized Cu values (Cu/Cu(TOR)) the two measured configuration differs from each other, hence not only the magnitude of the Cu but also the gradient of Cu are different between the two configurations.

Height	**Cu_train/Cu_smooth [-]**
TOR	1.85960
0.1xTOR	2.21660
0.15xTOR	2.18102
0.25xTOR	2.11479
0.5xTOR	2.00957
0.75xTOR	1.93077
1.25xTOR	1.76191
1.5xTOR	1.66749

Table 2: Comparison between the two configurations of the Cu average for the 2nd coach.

A direct comparison between the two configurations was done with the Cu average for the 2nd coach, the results are shown in Table 2. As expected the generic high-speed train configuration had a higher Cu average than the smooth generic high-speed train configuration. The reason for the higher Cu averages is simply the higher roughness on the underbelly of the generic high-speed train configuration. The largest difference was found close to the ground.

4.2 Velocity Profiles

For a better view of the velocity distribution over the gap (ground-train) velocity profiles were extracted for both configurations. For the front car, the 2 coaches and the tail car, each 7 velocity profiles were extracted and plotted with an offset in Fig. 9 and Fig. 10. The first profile for every coach (orange line 1,8,15,22 from the left in Fig. 9 and Fig 10) has an offset of 0, the second has an offset of 1 and so on until the seventh and the last velocity profile (offset of 6). The fourth velocity profile at every coach is in the middle of the coach, the three profiles to the left and to the right are distributed with a distance of Δx=0.04 m from each other. The regions closest to the train and the ground are chosen not to be plotted due to the reflections laser light sheet on the train model and on the ground.

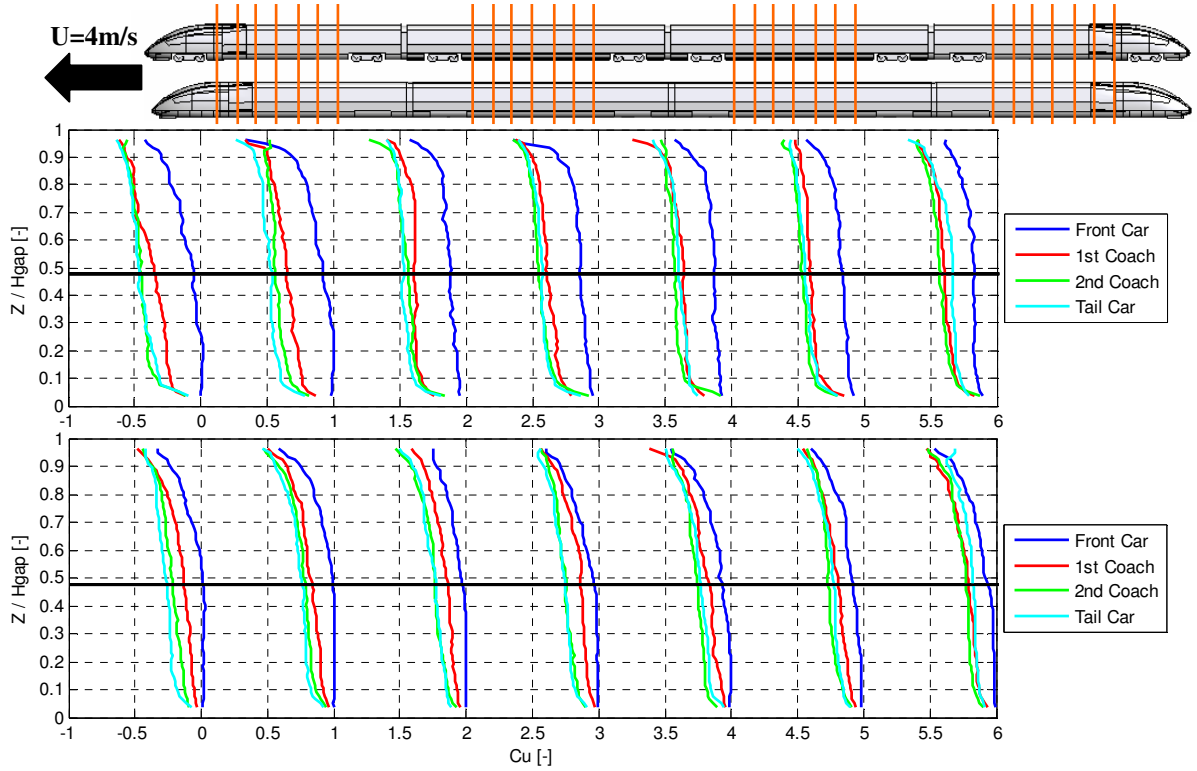

Figure 9: Comparison between the velocity profiles for the different coaches generic high-speed train configuration (upper plot) and the smooth generic high-speed train configuration (lower plot), the black solid horizontal line indicates the TOR and the orange lines on the trains above the plots shows the positions of the velocity profiles.

In Fig. 9 the velocity profiles from the front car, the 2 coaches and the tail car are plotted on top of each other for the generic high-speed train configuration (upper plot) and the smooth generic high-speed train configuration (lower plot). The velocity profiles shows the development of the flow underneath the both configurations, the flow is fully developed at the 2nd coach for both configurations since the differences between the velocity profiles for the 2nd coach (green) and the tail car (cyan) are small. Another indication that the flow is fully devel-

oped at the 2nd coach is the trend for the velocity profiles for the 1st coach (red). The profile difference between the 1st coach and the 2nd coach becomes smaller in the direction of the train model length (from left to right in Fig. 9). For the velocity profiles furthest to the right, a larger difference than before is found between the tail car (cyan) and the 2nd coach. This is probably the effects of the train model tail.

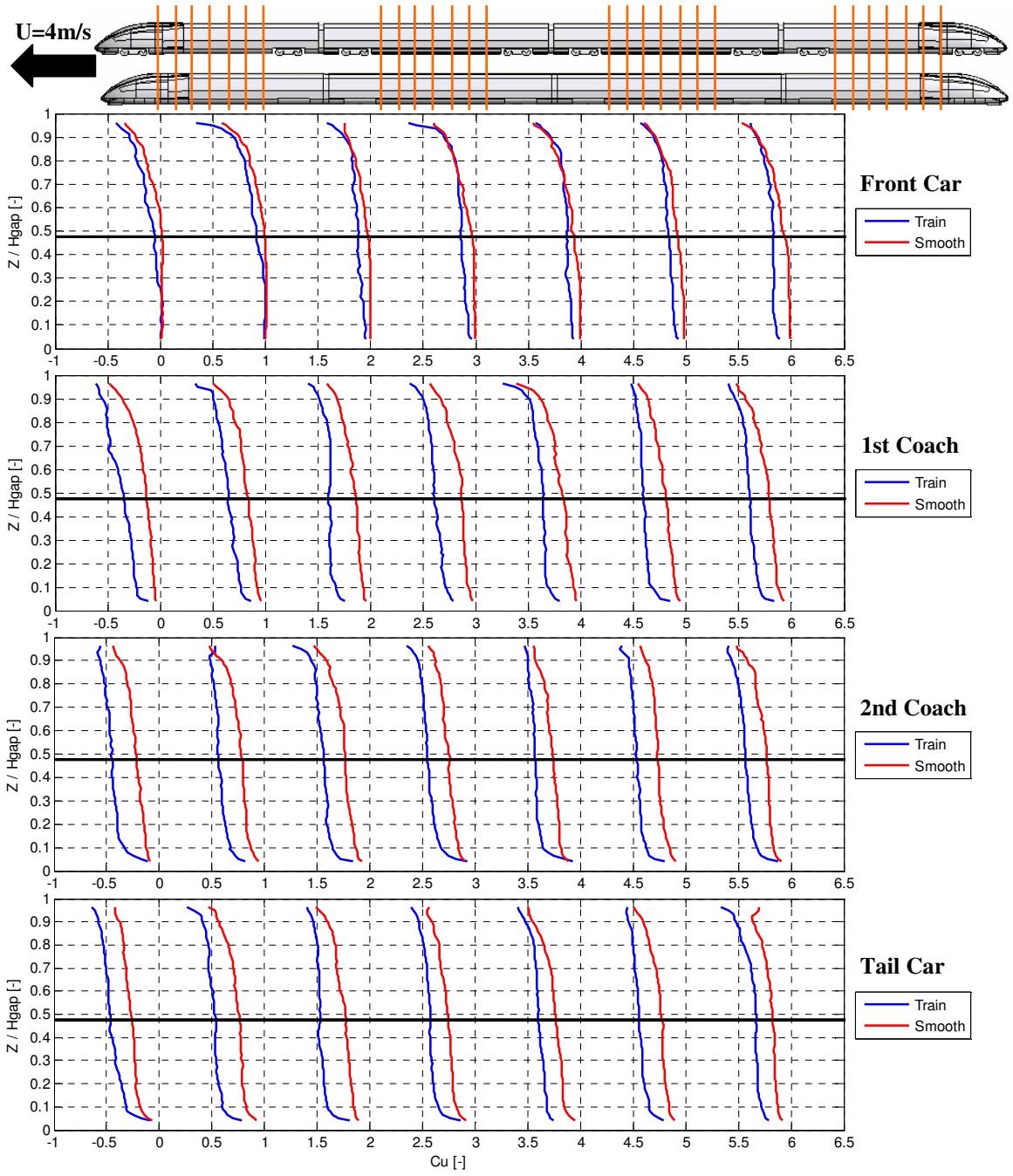

Figure 10: Comparison of the velocity profiles underneath the generic high-speed train configuration (blue) and the smooth generic high-speed train configuration (red), the black solid horizontal line indicates the TOR and the orange vertical lines on the trains above the plots shows the positions of the velocity profiles.

In Fig. 10 the velocity profiles for the two configurations are compared to each other for the front car, 1st coach, 2nd coach and the tail car. A clear difference between the two configurations can be seen for every velocity profile. It is only for the 1st and 2nd velocity profile for

the front car below Z/Hgap <0.3 where the profiles are hard to separate from each other. The Cu values close to the ground and the gradients are higher for the generic high-speed train configuration than for the smooth generic high-speed train configuration, hence the generic high-speed train configuration has a higher risk for ballast projection incidents. Another interesting observation is the similarities of the velocity profiles for the 1st coach, 2nd coach and the tail car between 0.2<Z/Hgap<0.7 where no major differences in the gradient can be seen.

4.3 Comparison to Full Scale Measurements

The PIV results from the water towing tank were compared to the full scale measurements on the Italian high-speed train ETR 500 [4], shown in Fig. 11. The down scaled train set had only 2 coaches except from the front car and the tail car where the ETR 500 had 12 coaches, therefore two comparison where done one for the beginning of the ETR 500 and the other one for the end. The length scale for the PIV results in the towing tank was transformed into full scale by multiplying it by the scale factor.

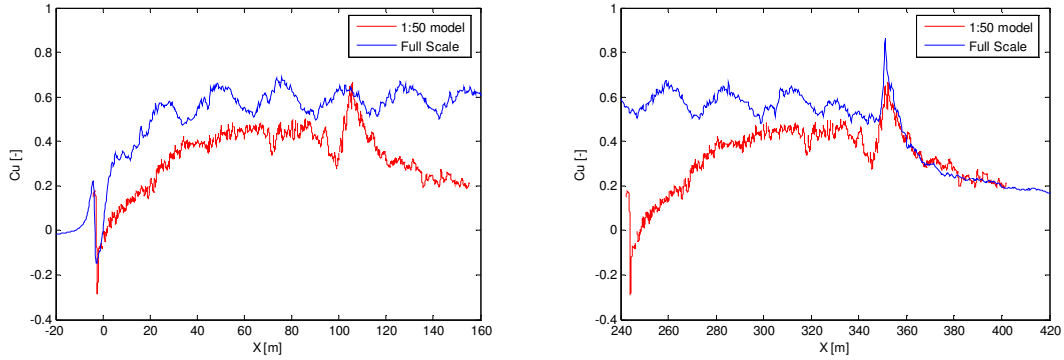

Figure 11: Comparison to full scale measurements [4].

For the generic high-speed train configuration the same structure of the flow field was found for the flow around the head and around the tail. The flow was fully developed at the beginning of the 2nd coach, which also was the case for the full scale measurement.

The down scaled train model never reached the same level of Cu as the full scale measurement. The reason for this is the simplified bogies that were used for the down scaled measurement which are completely smooth on the surface facing the ground, see Fig. 2. Hence the simplified bogies are aerodynamically better than the real bogies on a train where a lot of protruding objects exists (gear box, electrical motor, cables etc). The air can also flow into the bogie cut out and be accelerated by the train. The simplified bogies with a smooth surface shields the bogie cut out and are therefore aerodynamically better than the real ones.

Another parameter that plays an important role is the Reynolds number, also here a match could not be realized. For a full scale train with a speed of 270km/h a Re=15 Mio is reached, in the down scaled measurement in the water towing tank a maximum of Re=0.24 Mio was achieved.

5 CONCLUSIONS

- The PIV measurement technique is applicable to measure the flow field underneath a down scaled train model in a water towing tank.
- The flow field is fully developed at the beginning of the 2nd coach for both measured configurations. This also agrees with the full scale measurements.
- Underneath both configurations close to the ground the Cu is the dominant velocity, it is only at the head and at the tail where the vertical velocity (Cw) has to be taken into account.
- A clear difference between the generic high-speed train configuration and the smooth high-speed train configuration could be found, which was expected.
- The biggest difference between the velocity profiles for the two configurations was found close to the ground. However in the middle of the gap ($0.2<Z/Hgap<0.7$) for the 1st coach, 2nd coach and the tail car no major difference between the configurations could be seen, except for the magnitude of Cu.
- For the generic high-speed train configuration the same structures of the flow field was found for the flow around the head and around the tail as in the full scale measurements.
- To get more realistic data for the generic high-speed train configuration the simplified bogies should be exchanged with bogies with a higher degree of details.
- Important information can be extracted from down scaled measurements, however to extrapolate the results into full scale should be done with caution.

REFERENCES

[1] K. Shinojima. S*tudy on the Phenomena of Snow Adhering to and Dropping from Shinkansen Train, and the Countermeasures*. Quarterly Reports vol.25 No.2, p 41 – 44, 1984.

[2] L. Karlsson. Litteraturstudier till projektet stensprut X2000. Bombardier Transportation Internal Reports. Doc. Ref. No. RES/KBM/TR-91/066, 1991.

[3] P. Claus. AOA WP 1.2 Ballast Projection: Prestudy of Ballast Projection Incidents. 071119-AOA-WP1.2-Prestudy-V1.0, 2007.

[4] P. Deeg, M. Jönsson, H. J. Kaltenbach, M. Schober and M. Weise. Cross-Comparison of Measurement Techniques for the determination of train induced Aerodynamic Loads on the trackbed. Proceedings of the BBAA VI, Milano, Italy, July 20-24, 2008.

[5] H. Eckelmann. *Einführung in die Strömungsmeßtechnik*. B. G. Teubner, Stuttgart, Germany, 1997

[6] prEN 14067-6:2006 Railway Applications – Aerodynamics – Part 6: Requirements and test procedures for cross wind assessment. 2006.

[7] M. Raffel, C.E. Willert, S.T. Wereley and J. Kompenhans. *Particle Image Velocimetry 2nd ed.* Springer, Berlin, Germany, 2007.